AIMS Bioengineering, 10(3): 218–239.
DOI: 10.3934/bioeng.2023015
Received: 18 May 2023
Revised: 23 August 2023
Accepted: 23 August 2023
Published: 25 August 2023

http://www.aimspress.com/journal/Bioengineering

Research article

Real data-based optimal control strategies for assessing the impact of the Omicron variant on heart attacks

Fırat Evirgen[1], **Fatma Özköse**[2], **Mehmet Yavuz**[3,4,*] **and Necati Özdemir**[1]

[1] Department of Mathematics, Faculty of Science and Arts, Balıkesir University, 10100, Balıkesir, Turkey
[2] Erciyes University, Department of Mathematics, Faculty of Science, Kayseri, Turkey
[3] Centre for Environmental Mathematics, Faculty of Environment, Science and Economy, University of Exeter, TR10 9FE, United Kingdom
[4] Department of Mathematics and Computer Sciences, Faculty of Science, Necmettin Erbakan University, 42090 Konya, Turkey

* **Correspondence:** Email: M.Yavuz@exeter.ac.uk.

Abstract: This paper presents an investigation into the relationship between heart attacks and the Omicron variant, employing a novel mathematical model. The model incorporates two adjustable control parameters to manage the number of infected individuals and individuals with the Omicron variant. The study examines the model's positivity and boundedness, evaluates the reproduction number (R_0), and conducts a sensitivity analysis of the control parameters based on the reproduction number. The model's parameters are estimated using the widely utilized least squares curve fitting method, employing real COVID-19 cases from Türkiye. Finally, numerical simulations demonstrate the efficacy of the suggested controls in reducing the number of infected individuals and the Omicron population.

Keywords: Omicron variant; heart attack; parameter estimation; optimal control; sensitivity analysis

1. Introduction

The COVID-19 pandemic emerged on November 17, 2019 in Wuhan, the capital of the Hubei region of China. The disease emerged as a type of pneumonia that developed in humans without a specific reason, and as a result of research, a new coronavirus called SARS-CoV-2 was diagnosed. It has started to spread rapidly all over the world since the middle of January 2020. On March 11, 2020, the World Health Organization declared a global epidemic due to the rapidly spreading virus. As of May 15, 2022, while there were 521,097,997 confirmed cases and 475,547,947 recoveries in the world,

6,288,116 patients died due to the virus. There is some inconclusive evidence that the incubation period of the disease is between 2 and 27 days, during which time the virus is contagious. Symptoms of the disease include coughing, difficulty in breathing, high fever and loss of sense of smell. In addition, the virus can cause more deaths, especially in individuals with chronic diseases (https://covid19.who.int/).

As the virus continues to spread worldwide, many variants have emerged in this process. Among them, the fastest spreading Omicron variant (B.1.1.529) first appeared on 24 November 2021 in South Africa. Omicron comparison to the Delta variant multiplies approximately 70 times faster in the bronchi (lung and respiratory tract). However, the Omicron variant is 91% less deadly than the delta variant and has a 51% less risk of hospitalization. However, it is still seen as a risk in individuals with a chronic disorder or low immunity.

Although COVID-19 infection is seen as a respiratory disease, basically one third of coronavirus-related deaths occur due to heart-related causes. The COVID-19 virus itself basically occupies the vein that covers the inner surface of the vessel. Therefore, this virus can cause serious problems wherever there is a vein. The most important problem caused by the virus is that it causes intravascular coagulation. This situation, on the one hand, forms the basis of the involvements in the lungs, on the other hand, it appears as a factor that facilitates the heart attack [1–3].

When faced with an epidemic disease, state administrators and health institutions need to find answers to questions such as how the disease spreads and what are the factors in this spread in order to make the right decisions in the prevention of the disease. In this process, mathematical models play a key role. To date, many mathematical models related to infectious diseases and biology have been created. Among them, Naik et al. [4] investigated the dynamical properties of a discrete-time Bazykin-Berezovskaya prey-predator model characterized by a strong Allee effect and offer a detailed analysis of its dynamics. On the basis of the fluid model, Sene [5] discussed the impact of the second-grade parameter, as well as the Grashof number, on the velocity's dynamics. Sabbar [6] investigated the impact of jumps on an epidemic model which contains three intervention measures: media coverage, isolation, and medical therapy. In this research, the author provides sufficient criteria for asymptotic extinction and persistence. Hammouch et al. [7] provided a brunch of solutions to a chaotic system and synchronization. Especially, since the beginning of COVID-19, the disease has been attracting great interest of many scientists and contributed to the literature. Naik et al. [8], proposed a novel fractional-order epidemic model incorporating two distinct operators to analyze the transmission dynamics of the COVID-19 epidemic. Joshi et al. [9], presented a SIR model for Covid-19, incorporating the ABC derivative, to analyze the impacts of various factors, such as including face masks, social distancing, quarantine, etc. The proposed model employs a Beddington-DeAngelis infection rate and a Holling type-II treatment rate to assess the influence of different model parameters on the infected population. In [10], the main purpose of the authors is to conduct a comprehensive analysis of a fractional-order vaccination model designed specifically for COVID-19, taking into account the significant factor of environmental transmission. The investigation critically employs various tools derived from the field of fractional calculus to examine the intricate dynamics of the model and to gain deeper insights into the complex interactions between vaccination strategies and environmental factors in combating the spread of the virus. With all that, Ucar et al. [11] investigated the dynamics and numerical simulations of a smoking model by taking light, regular, and quit smokers into account. In another study [12], the authors introduced a dynamical HIV-1 model in the Caputo sense, incorporating the interplay among cancer cells, healthy CD4+T lymphocytes, and virus-infected CD4+T lymphocytes, resulting in the

emergence of chaotic dynamics. Modeling the dynamics of influenza A disease by incorporating the Caputo-Fabrizio (CF) fractional derivative operator is handled in [13]. Of particular significance in the model is the consideration of distinct contact rates between exposed and infected individuals, which contributes to a more accurate representation of the disease transmission process. Ucar et al. [14] considered an SAIDR-type model to examine the computer viruses dynamics. Elhia et al. [15] investigated the tuberculosis dynamics with multiple infectious compartments and time delays. In the paper [16], the co-dynamics of malaria and cholera are investigated within the framework of the Caputo-Fabrizio derivative. Additionally, the reader can refer to additional important contributions in this area by carefully reading the references [17].

A mathematical model can be improved by adding some meaningful parameters, allowing for the formulation of optimal control problems, and thus different strategies can be developed to assist in the prevention and treatment of diseases in the future. There are many studies in the literature that have been conducted on the optimal control of various diseases. The problem of fractional optimal control on a cancer model in which chemotherapy and immunotherapy drug concentrations are considered as control variables and the effect of obesity in this model is also investigated in [18]. Oncolytic virotherapy combined with chemotherapy is discussed in [19] for minimizing the cancer tumor cells. Various control strategies were examined by Akman et al. [20, 21] in an expanded tuberculosis model by adding three control parameters, such as distance control and prevention of treatment failures at home and in the hospital, which were added to the model. To minimize the deleterious impact of chemotherapy treatment, a fractional optimal control problem was designed and its effects on the growth of the pure tumor cell population were studied by Balenau et al. [22]. In [23], an optimal control problem is suggested with three control parameters for describing the dengue outbreak in Johor State, Malaysia. Some control approaches that include therapy for respiratory syncytial virus disease have been proposed by Jajarmi et al. [24] in the sense of fractional derivative. In the same way, in order to minimize the number of individuals who were exposed to HIV, four control parameters were considered in a fractional HIV transmission model by [25]. In the recent studies of Amenn et al. [26], two control parameters as vaccination and treatment were added to a fractional SIRV model designed for some infectious diseases and optimal treatment protocols were proposed. Elhia et al. [27] applied optimal control techniques to a SEIR tuberculosis disease model with time delay, three infectious compartments, and three controls. Some control approaches in a detailed variable-order fractional cancer treatment model consisting of 18 compartments were presented by Sweilam et al. [28]. In addition, transmission dynamics of echinococcosis and mumps virus and some treatment control strategies recommended for eradication of these diseases can be found in [29, 30], respectively. Especially, recently, there are studies on optimal control of COVID-19 and its co-infection [31–38].

The purpose of the study is initially to determine the parameters that play an important role in the transmission of COVID-19 and Omicron, and then to integrate the appropriate optimal control strategies into the model in order to predict and control the spread of the disease. In line with this target, we have proposed a model to investigate the impact of COVID-19 and the Omicron variant on the risk of a heart attack. In addition, two control variables are added to the mathematical model which is defined as self-isolation (u_1) and treatment (u_2). In this way, the effects of the added control mechanisms on the model have been examined. According to our knowledge, there is not an optimal control study in the literature that has been conducted to investigate the effects of the Omicron variant on heart attacks. First, we have proved the positivity and boundedness of the new model. Then, the

disease-free equilibrium point and the corresponding basic reproduction number are determined to examine the rate of the disease spread and its limit. Sensitivity analysis has been carried out in order to observe the effects of model and control parameters on the reproduction number. In addition, in order to obtain a more realistic model, the parameters used in the numerical simulation have been determined in the most appropriate way to the real COVID-19 data from Türkiye with the parameter estimation approach. As a final step, the maximum principle of Pontryagin is used to establish the necessary conditions to minimize the objective functional, which is designed for the optimal control problem. The solution of the optimal control problem has been performed numerically by the forward-backward sweep method, and thus the effectiveness of the created control strategies has been examined.

The paper is divided into the following sections: the new model that summarizes the relation between COVID-19, Omicron, and heart attack has been introduced in Section 2. Section 3 specifies the solution's positivity and boundedness. In addition, R_0 has been determined. The parameters in Section 4 have been used in the sensitivity analysis to calculate the impact on R_0. In Section 5, the parameter estimation approach is examined. In Section 6, the optimal control problem is created and the necessary and sufficient conditions for the minimization of the objective functional are expressed. Forward-backward sweep method has been utilized to examine the effects of the designed control approaches on the model variables according to the parameters in Table 1, in Section 7. Finally, Section 8 provides a synopsis of the current work.

2. Mathematical modelling

We can forecast the scope and severity of infectious diseases by utilizing mathematical models to depict them. Mathematical models can be used to create plans of action to remedy numerous diseases and stop their spread. Different mathematical models have been used to describe the COVID-19 pandemic. One of these models illustrates the severity of COVID-19's harmful effects on a number of other illnesses. Some of these models included vaccination, while others included the quarantine that was implemented to stop the transmission of the disease. A few models also depict COVID-19's impact on various illnesses, with chronic conditions like diabetes [39] being among the most significant. In this study, a model has been developed to investigate the harmful effects of COVID-19 and the Omicron variant on heart attack disease patients by taking into account the optimal control approaches. In the model, we adopt two controls as the self-isolation of infected individuals $u_1(t)$ and different types of treatment alternatives $u_2(t)$ such as drug, physiological therapy, etc.

Six subpopulations are considered in order to examine the transmission of COVID-19 with and without the Omicron variant as susceptible ($\mathcal{S}$), exposed ($\mathcal{E}$), infected without Omicron ($\mathcal{I}$), Omicron-infected ($\mathcal{O}$), recovered ($\mathcal{R}$), and heart attack ($\mathcal{H}$). The proposed integer-order model is as follows:

$$\begin{aligned}
\frac{d\mathcal{S}}{dt} &= \Lambda - (\mu+\gamma_1)\mathcal{S} - \beta_1\frac{\mathcal{S}\mathcal{E}}{\mathcal{N}} - \beta_2\frac{\mathcal{S}\mathcal{I}}{\mathcal{N}} - \beta_3\frac{\mathcal{S}\mathcal{O}}{\mathcal{N}},\\
\frac{d\mathcal{E}}{dt} &= \beta_1(1-\varepsilon_1-\varepsilon_2)\frac{\mathcal{S}\mathcal{E}}{\mathcal{N}} - (\mu+\alpha_1+\sigma)\mathcal{E},\\
\frac{d\mathcal{I}}{dt} &= \beta_1\varepsilon_1\frac{\mathcal{S}\mathcal{E}}{\mathcal{N}} + \beta_2\frac{\mathcal{S}\mathcal{I}}{\mathcal{N}} + \alpha_1\mathcal{E} - (\mu+\alpha_2+\delta_1+\delta_2+u_1)\mathcal{I},\\
\frac{d\mathcal{O}}{dt} &= \beta_1\varepsilon_2\frac{\mathcal{S}\mathcal{E}}{\mathcal{N}} + \beta_3\frac{\mathcal{S}\mathcal{O}}{\mathcal{N}} + \sigma\mathcal{E} - (\mu+\alpha_3+\delta_3+\delta_4+u_2)\mathcal{O},
\end{aligned} \tag{2.1}$$

$$\begin{aligned}\frac{d\mathcal{R}}{dt} &= \alpha_2\mathcal{I} + \alpha_3\mathcal{O} - \gamma_2\mathcal{R} - \mu\mathcal{R} + u_1\mathcal{I} + u_2\mathcal{O},\\ \frac{d\mathcal{H}}{dt} &= \gamma_1\mathcal{S} + \delta_2\mathcal{I} + \delta_4\mathcal{O} + \gamma_2\mathcal{R} - (\mu_2+\mu)\mathcal{H},\end{aligned}$$

with subject to the following initial conditions

$$\mathcal{S}(0) = \mathcal{S}_0 \geq 0, \mathcal{E}(0) = \mathcal{E}_0 \geq 0, \mathcal{I}(0) = \mathcal{I}_0 \geq 0, \mathcal{O}(0) = \mathcal{O}_0 \geq 0, \mathcal{R}(0) = \mathcal{R}_0 \geq 0, \mathcal{H}(0) = \mathcal{H}_0 \geq 0.$$

Table 1 provides the biological meanings of the values in the model (2.1).

Table 1. Parameters that were used in the numerical analysis and their values.

Par.	Meaning	Value	Source
Λ	Rate of recruitment	$2.9517e+03$	Estimated
μ	The natural death rate	$3.4857e-05$	Estimated
μ_2	The rate of people who die as a result of a heart attack	0.8000	Fitted
γ_1	The probability of having a heart attack in those who are susceptible	0.0247	Fitted
γ_2	The probability of having a heart attack in those who are recovered	0.6000	Fitted
δ_1	The mortality rate due to complications	0.1161	Fitted
δ_2	The probability of having a heart attack in those who are infected in I class	0.1085	Fitted
δ_3	The rate of fatalities from complications	0.5000	Fitted
δ_4	The probability of having a heart attack in those who are infected in O class	0.4000	Fitted
β_1	Disease transmission rate by contact with the E class	0.3963	Fitted
β_2	Disease transmission rate by contact with the I class	0.5000	Fitted
β_3	Disease transmission rate by contact with the O class	0.7000	Fitted
α_1	the fraction of COVID-19 infected people who are screened	0.0034	Fitted
α_2	The proportion of individuals that recovered from the I class	0.0994	Fitted
α_3	The proportion of individuals that recovered from the O class	0.7800	Fitted
σ	The screening rate of people infected with the Omicron variant	0.0664	Fitted
ε_1	Detection of infection with a non-Omicron variant	$1.0000e-04$	Fitted
ε_2	Detection of infection with an Omicron variant	$1.0000e-04$	Fitted

3. Positivity and boundedness of the solution

This section examines both the positivity and the boundedness of the solution which is given by model (2.1). Let $R^6_+ = \zeta(t) \in R^6 : \zeta(t) \geq 0$ and $\zeta(t) = [\mathcal{S}(t), \mathcal{E}(t), \mathcal{I}(t), \mathcal{O}(t), \mathcal{R}(t), \mathcal{H}(t)]^T$. We demonstrate the non-negativeness of the model (2.1) solution.

Theorem 1. *Along with the initial conditions, the solution of model (2.1) is bounded in* R^6_+.

Proof. Assuming positive invariance for the non-negative region R^6_+. We achieve the following using the system (2.1):

$$\begin{aligned}\mathcal{S}'|_{\mathcal{S}=0} &= \Lambda \geq 0,\\ \mathcal{E}'|_{\mathcal{E}=0} &= 0 \geq 0,\\ \mathcal{I}'|_{\mathcal{I}=0} &= \beta_1\varepsilon_1\frac{\mathcal{S}\mathcal{E}}{\mathcal{N}} + \alpha_1\mathcal{E} \geq 0,\end{aligned}$$

$$\begin{aligned} \mathcal{O}'|_{\mathcal{O}=0} &= \beta_1\varepsilon_2\frac{\mathcal{S}\mathcal{E}}{\mathcal{N}} + \sigma\mathcal{E} \geq 0, \\ \mathcal{R}'|_{\mathcal{R}=0} &= (\alpha_2 + u_1)\mathcal{I} + (\alpha_3 + u_2)\mathcal{O} \geq 0, \\ \mathcal{H}'|_{\mathcal{H}=0} &= \gamma_1\mathcal{S} + \delta_2\mathcal{I} + \delta_4\mathcal{O} + \gamma_2\mathcal{R} \geq 0. \end{aligned} \tag{3.1}$$

If $(\mathcal{S}(0), \mathcal{E}(0), \mathcal{I}(0), \mathcal{O}(0), \mathcal{R}(0), \mathcal{H}(0)) \in R_+^6$, then from the system (3.1), the hyperplanes $\mathcal{S} = 0, \mathcal{E} = 0, \mathcal{I} = 0, \mathcal{O} = 0, \mathcal{R} = 0$, and $\mathcal{H} = 0$ are an impassable barrier for the solution of model (2.1). This means that the region R_+^6 is a set that is positively invariant.

Theorem 2. *The region*
$\mathcal{P} = \{(\mathcal{S}(t), \mathcal{E}(t), \mathcal{I}(t), \mathcal{O}(t), \mathcal{R}(t), \mathcal{H}(t)) \in R_+^6, 0 < \mathcal{S}(t) + \mathcal{E}(t) + \mathcal{I}(t) + \mathcal{O}(t) + \mathcal{R}(t) + \mathcal{H}(t) \leq \frac{\Lambda}{\mu}\}$ *is a positive invariant set for the system* (2.1).

Proof. Based on model (2.1), we get $\mathcal{N}'(t) = \Lambda - \mu(\mathcal{S}(t) + \mathcal{E}(t) + \mathcal{I}(t) + \mathcal{O}(t) + \mathcal{R}(t) + \mathcal{H}(t)) - \mu_2\mathcal{H}(t) - \delta_1\mathcal{I}(t) - \delta_3\mathcal{O}(t)$.
This gives $\mathcal{N}'(t) \leq \Lambda - \mu\mathcal{N}(t)$. We get by applying the Laplace transform to the last equation $s\mathcal{N}(s) - \mathcal{N}(0) \leq \frac{\Lambda}{s} - \mu\mathcal{N}(s)$, which further gives $\mathcal{N}(s) \leq \frac{\Lambda}{s(s+\mu)} + \frac{\mathcal{N}(0)}{s+\mu}$. We deduce that if $(\mathcal{S}_0, \mathcal{E}_0, \mathcal{I}_0, \mathcal{O}_0, \mathcal{R}_0, \mathcal{H}_0) \in R_+^6$, then $\mathcal{N}(t) \leq \frac{\Lambda}{\mu}$. This implies that the total population $\mathcal{N}(t)$ is bounded, thus, $\mathcal{S}(t), \mathcal{E}(t), \mathcal{I}(t), \mathcal{O}(t), \mathcal{R}(t)$ *and* $\mathcal{H}(t)$ are bounded.

Basic reproduction number

The disease transmission coefficient ("R_0") is determined for the local stability of the disease-free equilibrium $\overline{DFE}$ using the next generation matrix method (NGMM) [40,41]. R_0 represents the extent of the virus's dissemination or the number of persons who can become infected with it. Biologically, if $R_0 < 1$ then the infection will die out, if $R_0 > 1$, the disease remains in the community. In order to determine R_0, the right side of the model (2.1) is considered as $\mathcal{F}$-$\mathcal{V}$, where $\mathcal{F}$ and $\mathcal{V}$ demonstrate the transmission part and the transition part, respectively.

$$\mathcal{F} = \begin{pmatrix} 0 \\ \beta_1\frac{\mathcal{S}^0\mathcal{E}^0}{\mathcal{N}} \\ \beta_2\frac{\mathcal{S}^0\mathcal{I}^0}{\mathcal{N}} \\ \beta_3\frac{\mathcal{S}^0\mathcal{O}^0}{\mathcal{N}} \\ 0 \\ 0 \end{pmatrix},$$

and

$$\mathcal{V} = \begin{pmatrix} (\mu + \gamma_1)\mathcal{S}^0 + \beta_1\frac{\mathcal{S}^0\mathcal{E}^0}{\mathcal{N}} + \beta_2\frac{\mathcal{S}^0\mathcal{I}^0}{\mathcal{N}} + \beta_3\frac{\mathcal{S}^0\mathcal{O}^0}{\mathcal{N}} \\ \beta_1(\varepsilon_1 + \varepsilon_2)\frac{\mathcal{S}^0\mathcal{E}^0}{\mathcal{N}} + (\mu + \alpha_1 + \sigma)\mathcal{E}^0 \\ -\beta_1\varepsilon_1\frac{\mathcal{S}^0\mathcal{E}^0}{\mathcal{N}} - \alpha_1\mathcal{E}^0 + (\mu + \alpha_2 + u_1 + \delta_1 + \delta_2)\,\mathcal{I}^0 \\ -\beta_1\varepsilon_2\frac{\mathcal{S}^0\mathcal{E}^0}{\mathcal{N}} - \sigma\mathcal{E}^0 + (\mu + \alpha_3 + u_2 + \delta_3 + \delta_4)\,\mathcal{O}^0 \\ -\alpha_2\mathcal{I}^0 - \alpha_3\mathcal{O}^0 + \gamma_2\mathcal{R}^0 + \mu\mathcal{R}^0 - u_1\mathcal{I}^0 - u_2\mathcal{O}^0 \\ -\gamma_1\mathcal{S}^0 - \delta_2\mathcal{I}^0 - \delta_4\mathcal{O}^0 - \gamma_2\mathcal{R}^0 + (\mu_2 + \mu)\mathcal{H}^0 \end{pmatrix}.$$

By utilizing the NGMM [40, 41], the matrices $\mathbb{F}$ and $\mathbb{V}$ at $\overline{DFE} = (\mathcal{S}^0, \mathcal{E}^0, \mathcal{I}^0, \mathcal{O}^0, \mathcal{R}^0, \mathcal{H}^0) =$

$\left(\frac{\Lambda}{\mu+\gamma_1}, 0, 0, 0, 0, \frac{\gamma_1\Lambda}{(\mu+\gamma_1)(\mu+\mu_2)}\right)$ are obtained by $\mathbb{F} = \left[\frac{\partial \mathcal{F}_x(\overline{DFE})}{\partial t_y}\right]$ and $\mathbb{V} = \left[\frac{\partial \mathcal{V}_x(\overline{DFE})}{\partial t_y}\right]$, $1 \le x, y \le 3$. This implies,

$$\mathbb{F} = \begin{pmatrix} \beta_1\frac{S^0}{N} & 0 & 0 \\ 0 & \beta_2\frac{S^0}{N} & 0 \\ 0 & 0 & \beta_3\frac{S^0}{N} \end{pmatrix},$$

$$\mathbb{V} = \begin{pmatrix} \beta_1(\varepsilon_1+\varepsilon_2)\frac{S^0}{N} + (\alpha_1+\mu+\sigma) & 0 & 0 \\ -\alpha_1 - \beta_1\varepsilon_1\frac{S^0}{N} & \delta_1+\delta_2+\mu+u_1+\alpha_2 & 0 \\ -\sigma - \beta_1\varepsilon_2\frac{S^0}{N} & 0 & \alpha_3+\delta_3+\delta_4+\mu+u_2 \end{pmatrix}.$$

R_0 is computed using the spectral radius of the matrix $\left(\mathbb{F}\mathbb{V}^{-1}\right)$ at $\overline{DFE}$, which is represented by three situation, R_{01}, R_{02} and R_{03}:

$$\begin{aligned} R_{01} &= \frac{\Lambda\beta_1}{\Lambda\beta_1(\varepsilon_1+\varepsilon_2) + \mathcal{N}(\mu^2+\alpha_1\gamma_1+\alpha_1\mu+\gamma_1\mu+\gamma_1\sigma+\mu\sigma)}, \\ R_{02} &= \frac{\Lambda\beta_2}{\mathcal{N}(\gamma_1+\mu)(\alpha_2+\delta_1+\delta_2+\mu+u_1)}, \\ R_{03} &= \frac{\Lambda\beta_3}{\mathcal{N}(\gamma_1+\mu)(\alpha_3+\delta_3+\delta_4+\mu+u_2)}, \end{aligned}$$

in which

$$R_0 = \max\left[R_{01}, R_{02}, R_{03}\right]. \tag{3.2}$$

4. Sensitivity analysis of R_0

The goal of this part is to investigate the sensitivity of R_{01}, R_{02}, and R_{03} according to the reproduction number-influencing parameters. In these analyses, only the effects of $\beta_1, \beta_2, \beta_3, \varepsilon_1, u_1$ and u_2 parameters on the relevant reproduction number values were taken into account. We have applied the same method as in [42] and get the following:

$$\begin{aligned} \frac{\partial R_{01}}{\partial\beta_1} &= \frac{\Lambda}{\Lambda(\varepsilon_1+\varepsilon_2) + \mathcal{N}(\mu^2+\alpha_1\gamma_1+\alpha_1\mu+\gamma_1\mu+\gamma_1\sigma+\mu\sigma)} > 0, \\ \frac{\partial R_{01}}{\partial\sigma} &= -\frac{\Lambda\beta_1\mathcal{N}(\gamma_1+\mu)}{\left(\Lambda(\varepsilon_1+\varepsilon_2) + \mathcal{N}(\mu^2+\alpha_1\gamma_1+\alpha_1\mu+\gamma_1\mu+\gamma_1\sigma+\mu\sigma)\right)^2} < 0, \\ \frac{\partial R_{02}}{\partial\beta_2} &= \frac{\Lambda}{\mathcal{N}(\gamma_1+\mu)(\alpha_2+\delta_1+\delta_2+\mu+u_1)} > 0, \\ \frac{\partial R_{02}}{\partial u_1} &= -\frac{\Lambda\beta_2}{\mathcal{N}(\gamma_1+\mu)(\alpha_2+\delta_1+\delta_2+\mu+u_1)^2} < 0, \\ \frac{\partial R_{03}}{\partial\beta_3} &= \frac{\Lambda}{\mathcal{N}(\gamma_1+\mu)(\alpha_3+\delta_3+\delta_4+\mu+u_2)} > 0, \\ \frac{\partial R_{03}}{\partial u_2} &= -\frac{\Lambda\beta_3}{\mathcal{N}(\gamma_1+\mu)(\alpha_3+\delta_3+\delta_4+\mu+u_2)^2} < 0. \end{aligned}$$

In the sensitivity analysis, one can see that the values of R_{01} and R_{02} increase and decrease in proportion to the growth of β_1, σ and β_2, u_1 values, respectively. Similarly, the value of R_{03} increases and

decreases in proportion to the growth of β_3 and u_2 values. In addition, Figure 1 shows the effects of the parameters considered in the analysis on the relevant reproduction numbers within the determined limitations. When the analyses and visuals are studied, it is concluded that reasonable steps should be done to decrease the spread of the disease by minimizing the parameters that cause the derivative of reproduction numbers to be positive and maximizing the factors that cause it to be negative.

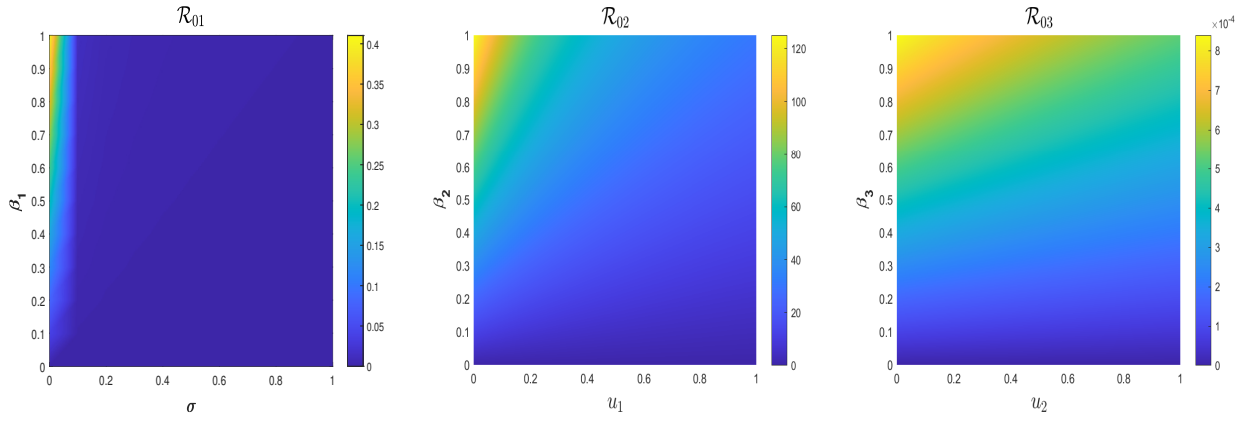

(a) **(b)** **(c)**

Figure 1. Sensitivity analysis of reproduction numbers according to model and control parameters.

5. Estimating of model parameters

Using the parameter estimation (PE) methodology, which is gaining a growing amount of popularity in the last few years, we can generate the curve that fits the real data the best while identifying the parameter values that are closest to the real data. In order to provide a better understanding of how this method works, the following algorithm can be used

- Locate the coefficients c that resolve the issue $\min_c \|X(c, cdata) - ydata\|_2^2 = \min_c \sum_i (X(c, cdata_i) - ydata_i)^2$, given input data $cdata$, and the observed output $ydata$, where $cdata$ and $ydata$ are matrices or vectors, and $X(c, cdata)$ is a similar-sized matrix-valued or vector-valued function to $ydata$.
- Lower and upper bounds, denoted by lb and ub, can be determined if there are boundaries. The arguments c, lb, and ub can be vectors or matrices.
- The following vector-valued function must be calculated using the user-defined function; the MATLAB routine *lsqcurvefit* only provides a minimal user interface for data-fitting concerns.

$$X(c, cdata) = \begin{bmatrix} X(c, cdata(1)) \\ X(c, cdata(2)) \\ X(c, cdata(3)) \\ \vdots \\ X(c, cdata(k)) \end{bmatrix}.$$

The heart attack and COVID-19 interaction model we built has a total of 18 parameter values. Utilizing actual COVID-19 data from Türkiye, we fitted 16 parameters to the objectives of the aforementioned algorithm (https://covid19.saglik.gov.tr/), and by using Türkiye's current average lifespan of 78.6 years and its entire population of 84, 680, 273 (https://www.worldometers.info/world-population/turkey-population/), we estimated the recruitment rate Λ and the natural death rate μ. If the initial conditions are taken into account as the entire population of Türkiye and the initially exposed individuals $\mathcal{E}(0) = 65,000$, since $\mathcal{N}(0) = \mathcal{S}(0)+\mathcal{E}(0)+\mathcal{I}(0)+\mathcal{O}(0)+\mathcal{R}(0)+\mathcal{H}(0)$, $\mathcal{S}(0) = 69,628,891$, $\mathcal{O}(0) = 1,300$, $\mathcal{I}(0) = 36,731$, other remaining populations are calculated as $\mathcal{R}(0) = 14,947,920$, and $\mathcal{H}(0) = 431$. As can be seen in Table 1, the parameter values that were used in the modeling process are listed along with the best-fit values that were obtained using the Least squares Curve fitting Method (LCM). Along with this, by utilizing real data in Türkiye from January 1, 2022, to March 31, 2022, the second infectious rate $R_{01} = 0.0080$, $R_{02} = 0.0022$, and $R_{03} = 5.8717e-04$ have been computed. The real COVID-19 cases are shown in Figure 2 by the red-filled circles, and the model's best-fitting curve is shown by the blue solid line.

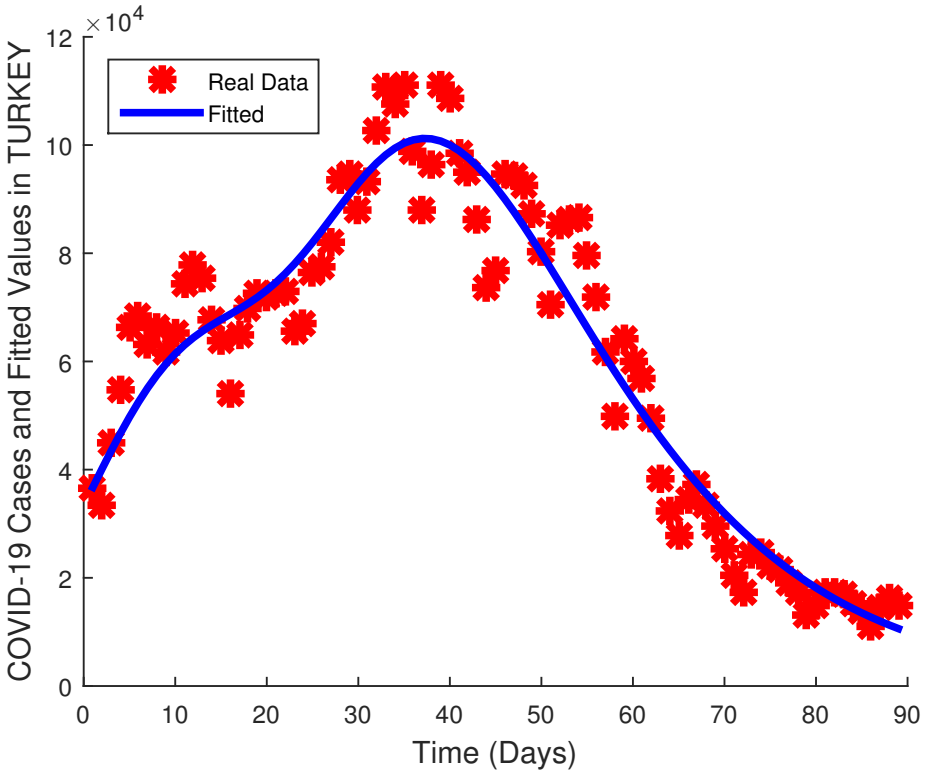

Figure 2. Real COVID-19 cases and the best-fitted curve in Türkiye from January 1, 2022, to March 31, 2022.

In order to assess the model parameters, we computed the absolute relative error values between the curve fitted in Figure 2 and the actual Covid-19 data, taking into account the progression of time. Figure 3 presents these error values, which indicate the level of agreement between the model and the real data. Notably, the fitted model parameters obtained from Figure 3 exhibit biological significance and inspire confidence in their validity.

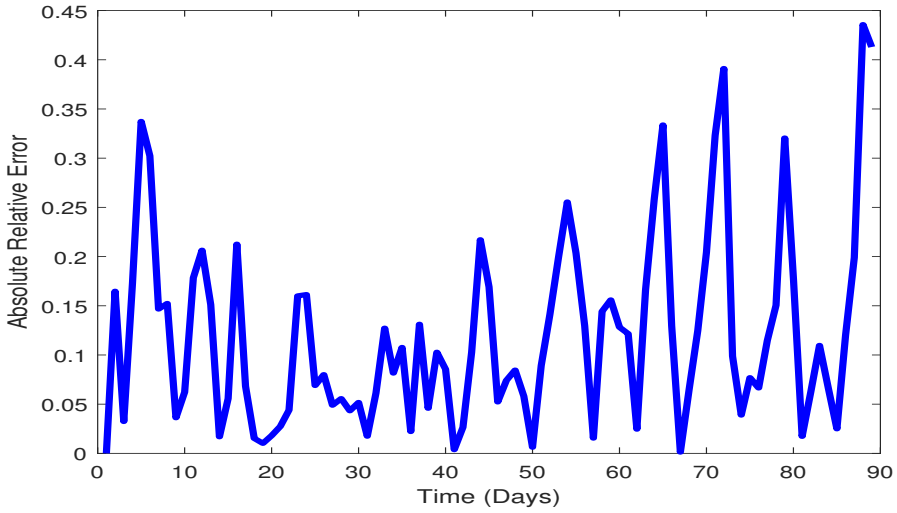

Figure 3. The absolute relative error values for model parameters.

In addition, statistical analyses were carried out in order to assess the reliability of the parameter values obtained on the basis of the simulation results. As a result of these analyses, a confidence interval (CI) was calculated based on the confidence level of each parameter estimate. The confidence intervals provide valuable information on the statistical precision of the parameter estimates. The calculated confidence intervals were obtained using a 99% confidence level and express how certain or uncertain each parameter estimate is at a given confidence level. This information allows us to understand the reliability of the simulation results in a more holistic way. The details of the confidence interval calculations are shown in Table 2.

Table 2. Confidence intervals calculated at 99% confidence level for the fitted parameters of model (2.1).

Parameter	CI Lower Bound	CI Upper Bound	Parameter	CI Lower Bound	CI Upper Bound
μ_2	0.322727	1.010640	β_2	0.500000	0.500000
γ_1	0.024653	0.024654	β_3	0.700000	0.700000
γ_2	0.242060	0.757974	α_1	0.003442	0.003442
δ_1	0.107950	0.153416	α_2	0.061371	0.103206
δ_2	0.086821	0.135284	α_3	0.780000	0.780000
δ_3	0.500000	0.500000	σ	0.066363	0.066363
δ_4	0.400000	0.400000	ε_1	0.000100	0.000100
β_1	0.396254	0.396255	ε_2	0.000100	0.000100

The confidence intervals obtained as a result of the conducted statistical analyses have been made more meaningful by considering only the 30 simulation values that are in line with Figure 2. An analysis of Table 2 shows that the lower and upper limits of the confidence intervals of some model parameters are almost equal. This indicates that the estimation obtained from the analysis is close to the real value of the model parameter. In addition, for the other model parameters, confidence intervals have been statistically obtained at the 99% confidence level, where the real value of the prediction is probably located.

6. Optimal control of the model

To reduce the number of COVID-19 patients without the Omicron variant as well as those with the Omicron variant in this section, we have introduced two time-dependent control parameters, $u_1(t)$ as self-isolation and $u_2(t)$ as treatment, to the model (2.1) based on the input data. On the basis of this, we suggest the optimal control problem (OCP)

$$\min_{(u_1(t),u_2(t))\in U_{ad}} J(u_1(t), u_2(t)) = \int_0^T \left(\epsilon_1 \mathcal{I}(t) + \epsilon_2 \mathcal{O}(t) + \frac{\epsilon_3}{2} u_1^2(t) + \frac{\epsilon_4}{2} u_2^2(t)\right) dt, \tag{6.1}$$

governed by the system (2.1) with the set of Lebesgue measurable admissible control given by

$$U_{ad} = \{u_1(t), u_2(t) \mid 0 \le u_1(t), u_2(t) \le 1,\ t \in [0, T]\},$$

where ϵ_i, $i = 1, 2, 3, 4$ represents the relative costs of the infected class, Omicron class, and associated control strategies, respectively. For the optimal control problem we are considering, the Lagrangian function L can be defined as follows:

$$L(\mathcal{S}, \mathcal{E}, \mathcal{I}, \mathcal{O}, \mathcal{R}, \mathcal{H}, u_1, u_2) = \epsilon_1 \mathcal{I}(t) + \epsilon_2 \mathcal{O}(t) + \frac{\epsilon_3}{2} u_1^2(t) + \frac{\epsilon_4}{2} u_2^2(t).$$

The cost functional $J(u_1(t), u_2(t))$ is minimized here by considering some constraints that are defined on the control variables $u_1(t)$ and $u_2(t)$. As a result of minimizing the cost functional, both the reduction of diseased individuals with COVID-19 $\mathcal{I}(t)$ and Omicron variants $\mathcal{O}(t)$, as well as the cost of implementing control strategies, are improved. In other words, we determine the solution of (2.1) as $(\mathcal{S}^*(t), \mathcal{E}^*(t), \mathcal{I}^*(t), \mathcal{O}^*(t), \mathcal{R}^*(t), \mathcal{H}^*(t))$ associated with the optimal control $\left(u_1^*(t), u_2^*(t)\right) \in U_{ad}$ so that

$$J\left(u_1^*(t), u_2^*(t)\right) = \min_{(u_1(t),u_2(t))\in U_{ad}} J(u_1(t), u_2(t)),$$

is reached.

Before giving the necessary conditions, let's first prove that there exists the $\left(u_1^*, u_2^*\right)$ optimal control pair for which the cost functional J is minimized in a finite period of time.

Theorem 3. *The $\left(u_1^*, u_2^*\right) \in U_{ad}$ optimal control pair exists such that $J(u_1^*, u_2^*) = \min J(u_1, u_2)$, solution to optimal control problem (6.1).*

Proof. The following conditions must be fulfilled in order to demonstrate the solution's existence:

(1) The admissible control set U_{ad} and the state solutions of (2.1) is nonempty.
(2) The admissible control set U_{ad} is both closed and convex and in addition, the state system can be described as a linear function of the control variables with coefficients that are dependent on time as well as state variables.
(3) The Lagrange function L in (6.1) is convex on the admisible control set U_{ad} and $L(\mathcal{S}, \mathcal{E}, \mathcal{I}, \mathcal{O}, \mathcal{R}, \mathcal{H}, u_1, u_2) \ge h(u_1, u_2)$, where $h(u_1, u_2)$ is continuous and $|(u_1, u_2)|^{-1} h(u_1, u_2) \to \infty$ whenever $|(u_1, u_2)| \to \infty$, with $|.|$ the $L^2(0, T)$ norm.

The solutions of the system (2.1) are bounded for each of the control variables u_1 and u_2 in the set U_{ad}, and the right-hand side satisfies the Lipschitz condition with regard to the state variables. So, condition (1) is satisfied by using the Picard-Lindelöf theorem [43]. The admissible control set U_{ad} is closed and convex by its definition. The model system (2.1) is linear in the control variables u_1 and u_2 with the coefficients depending on the state variables. Thus, condition (2) is held. Lastly, due to the fact that the control variables u_1 and u_1 are in quadratic nature, the Lagrange function L is convex. We have $L(\mathcal{S},\mathcal{E},\mathcal{I},\mathcal{O},\mathcal{R},\mathcal{H},u_1,u_2) \geq \frac{\epsilon_3}{2}u_1^2(t) + \frac{\epsilon_4}{2}u_2^2(t)$. Let $c = min(\epsilon_3,\epsilon_4) > 0$ and $h(u_1,u_2) = c\left(u_1^2 + u_2^2\right)$. In this case, condition (3) is also met as well. As a result, from [44], there exists a control pair $\left(u_1^*, u_2^*\right)$, minimizing the cost functional J.

Using the Maximum Principle of Pontryagin [45], we can now obtain the necessary conditions for the OCP (6.1). In order to do so, we define the Hamiltonian in the following way:

$$\begin{aligned}
&H(\mathcal{S}(t),\mathcal{E}(t),\mathcal{I}(t),\mathcal{O}(t),\mathcal{R}(t),\mathcal{H}(t),u_1(t),u_2(t))\\
&\quad = L(\mathcal{S}(t),\mathcal{E}(t),\mathcal{I}(t),\mathcal{O}(t),\mathcal{R}(t),\mathcal{H}(t),u_1(t),u_2(t))\\
&\quad + \lambda_1\left(\Lambda - (\mu+\gamma_1)\mathcal{S}(t) - \beta_1\frac{\mathcal{S}(t)\mathcal{E}(t)}{\mathcal{N}(t)} - \beta_2,\frac{\mathcal{S}(t)\mathcal{I}(t)}{\mathcal{N}(t)} - \beta_3\frac{\mathcal{S}(t)\mathcal{O}(t)}{\mathcal{N}(t)}\right)\\
&\quad + \lambda_2\left(\beta_1(1-\varepsilon_1-\varepsilon_2)\frac{\mathcal{S}(t)\mathcal{E}(t)}{\mathcal{N}(t)} - (\mu+\alpha_1+\sigma)\mathcal{E}(t)\right)\\
&\quad + \lambda_3\left(\beta_1\varepsilon_1\frac{\mathcal{S}(t)\mathcal{E}(t)}{\mathcal{N}(t)} + \beta_2\frac{\mathcal{S}(t)\mathcal{I}(t)}{\mathcal{N}(t)} + \alpha_1\mathcal{E}(t) - (\mu+\alpha_2+\delta_1+\delta_2+u_1(t))\,\mathcal{I}(t)\right)\\
&\quad + \lambda_4\left(\beta_1\varepsilon_2\frac{\mathcal{S}(t)\mathcal{E}(t)}{\mathcal{N}(t)} + \beta_3\frac{\mathcal{S}(t)\mathcal{O}(t)}{\mathcal{N}(t)} + \sigma\mathcal{E}(t) - (\mu+\alpha_3+\delta_3+\delta_4+u_2(t))\mathcal{O}(t)\right)\\
&\quad + \lambda_5(u_1(t)\,\mathcal{I}(t) + u_2(t)\,\mathcal{O}(t) + \alpha_2\mathcal{I}(t) + \alpha_3\mathcal{O}(t) - \mu\mathcal{R}(t) - \gamma_3\mathcal{R}(t))\\
&\quad + \lambda_6(\gamma_1\mathcal{S}(t) + \delta_2\mathcal{I}(t) + \delta_4\mathcal{O}(t) + \gamma_3\mathcal{R}(t) - (\mu_2+\mu)\,\mathcal{H}(t))\\
&\quad + \lambda_7(\Lambda - \mu_2\mathcal{H}(t) - \delta_1\mathcal{I}(t) - \mu\mathcal{N}(t) - \delta_3\mathcal{O}(t)),
\end{aligned} \tag{6.2}$$

where $\lambda_i(t)$, $1 \leq i \leq 7$ are the adjoint variables such that

$$\begin{aligned}
&\dot{\lambda}_1 = -\frac{\partial H}{\partial \mathcal{S}},\ \ \dot{\lambda}_2 = -\frac{\partial H}{\partial \mathcal{E}},\ \ \dot{\lambda}_3 = -\frac{\partial H}{\partial \mathcal{I}},\ \ \dot{\lambda}_4 = -\frac{\partial H}{\partial \mathcal{O}},\\
&\dot{\lambda}_5 = -\frac{\partial H}{\partial \mathcal{R}},\ \ \dot{\lambda}_6 = -\frac{\partial H}{\partial \mathcal{H}},\ \ \dot{\lambda}_7 = -\frac{\partial H}{\partial \mathcal{N}},
\end{aligned}$$

with the transversality conditions $\lambda_i(T) = 0$ for $1 \leq i \leq 7$. Optimal controls $(u_1(t), u_2(t))$ are obtained by the following relations

$$\begin{aligned}
\frac{\partial H}{\partial u_1} &= \epsilon_3 u_1(t) - \lambda_3\mathcal{I}(t) + \lambda_5\mathcal{I}(t) = 0,\\
\frac{\partial H}{\partial u_2} &= \epsilon_4 u_2(t) - \lambda_4\mathcal{O}(t) + \lambda_5\mathcal{O}(t) = 0.
\end{aligned}$$

Then, in order to arrive at the optimality conditions, we use the restrictions on u_i, $i = 1, 2$. The analysis presented above can be condensed into the theorem given below.

Theorem 4. *Let* $(\mathcal{S}^*(t), \mathcal{E}^*(t), \mathcal{I}^*(t), \mathcal{O}^*(t), \mathcal{R}^*(t), \mathcal{H}^*(t))$ *represent the optimal state solutions for the system (2.1), and* $\left(u_1^*, u_2^*\right) \in U_{ad}$ *represent the optimal control pair which is minimizing the objective functional (6.1). Then, there are adjoint variables* λ_i, $1 \le i \le 7$ *that provide*

$$
\begin{aligned}
\dot{\lambda}_1(t) &= -\lambda_1\left(-\mu+\gamma_1-\beta_1\frac{\mathcal{E}}{\mathcal{N}}-\beta_2,\frac{\mathcal{I}}{\mathcal{N}}-\beta_3\frac{\mathcal{O}}{\mathcal{N}}\right)-\lambda_2\beta_1(1-\varepsilon_1-\varepsilon_2)\frac{\mathcal{E}}{\mathcal{N}}-\lambda_3\left(\beta_1\varepsilon_1\frac{\mathcal{E}}{\mathcal{N}}+\beta_2\frac{\mathcal{I}}{\mathcal{N}}\right)\\
&\quad-\lambda_4\left(\beta_1\varepsilon_2\frac{\mathcal{E}}{\mathcal{N}}+\beta_3\frac{\mathcal{O}}{\mathcal{N}}\right)-\lambda_6\gamma_1,\\
\dot{\lambda}_2(t) &= \lambda_1\beta_1\frac{\mathcal{S}}{\mathcal{N}}-\lambda_2\left(\beta_1(1-\varepsilon_1-\varepsilon_2)\frac{\mathcal{S}}{\mathcal{N}}-\mu-\alpha_1-\sigma\right)-\lambda_3\left(\beta_1\varepsilon_1\frac{\mathcal{S}}{\mathcal{N}}+\alpha_1\right)-\lambda_4\left(\beta_1\varepsilon_2\frac{\mathcal{S}}{\mathcal{N}}+\sigma\right),\\
\dot{\lambda}_3(t) &= -\epsilon_1+\lambda_1\beta_2\frac{\mathcal{S}}{\mathcal{N}}-\lambda_3\left(\beta_2\frac{\mathcal{S}}{\mathcal{N}}-\mu-\alpha_2-\delta_1-\delta_2-u_1\right)-\lambda_5(u_1+\alpha_2)-\lambda_6\delta_2+\lambda_7\delta_1,\\
\dot{\lambda}_4(t) &= -\epsilon_2+\lambda_1\beta_3\frac{\mathcal{S}}{\mathcal{N}}-\lambda_4\left(\beta_3\frac{\mathcal{S}}{\mathcal{N}}-\mu-\alpha_3-\delta_3-\delta_4-u_2\right)-\lambda_5(u_2+\alpha_3)-\lambda_6\delta_4+\lambda_7\delta_3,\\
\dot{\lambda}_5(t) &= \lambda_5(\mu+\gamma_3)-\lambda_6\gamma_3,\\
\dot{\lambda}_6(t) &= \lambda_6(\mu+\mu_2)+\lambda_7\mu_2,\\
\dot{\lambda}_7(t) &= -\lambda_1\left(\beta_1\frac{\mathcal{SE}}{\mathcal{N}^2}+\beta_2\frac{\mathcal{SI}}{\mathcal{N}^2}+\beta_3\frac{\mathcal{SO}}{\mathcal{N}^2}\right)+\lambda_2\beta_1(1-\varepsilon_1-\varepsilon_2)\frac{\mathcal{SE}}{\mathcal{N}^2}+\lambda_3\left(\beta_1\varepsilon_1\frac{\mathcal{SE}}{\mathcal{N}^2}+\beta_2\frac{\mathcal{SI}}{\mathcal{N}^2}\right)\\
&\quad+\lambda_4\left(\beta_1\varepsilon_2\frac{\mathcal{SE}}{\mathcal{N}^2}+\beta_3\frac{\mathcal{SO}}{\mathcal{N}^2}\right)+\lambda_7\mu,
\end{aligned}
\tag{6.3}
$$

with the tranversality conditions $\lambda_i(T) = 0$ *for* $1 \le i \le 7$. *Furthermore, the following properties hold:*

$$
\begin{aligned}
u_1 &= min\left(max\left(\mathcal{I}^*(\lambda_3-\lambda_5)\epsilon_3^{-1},0\right),1\right),\\
u_2 &= min\left(max\left(\mathcal{O}^*(\lambda_4-\lambda_5)\epsilon_4^{-1},0\right),1\right).
\end{aligned}
\tag{6.4}
$$

7. Numerical simulations and discussion

In the literature, there are a variety of methods that can be used to solve problems of optimal control such as the Forward-Backward Sweep (FBS) method, total-enumeration method, or linear programming method. Here, we present the numerical solution to model (2.1) based on the FBS method [46] and the values in Table 1 as inputs for the numerical solution. In this method, the system's of state variables (2.1) have been solved forward in time and the system's of co-state variables (6.3) have been solved backward in time by using the well-known fourth-order Runge-Kutta method. As a result of numerical simulations, the effects of control parameters on the dynamics of populations who have been infected with COVID-19 and the Omicron variant have been investigated. For this investigation, model parameter values have been estimated with the real data from Türkiye between January 1 and March 31, 2022.

In numerical solutions of optimal control problem, since the cost of treatment of Omicron individuals is much more than the cost of self-isolation, we take the weight constants in cost functional (6.1) as $\epsilon_2 > \epsilon_1$ and $\epsilon_4 > \epsilon_3$.

In Figure 4, it is seen that there has been an increase in the number of susceptible individuals in the case of controls. This increase can be interpreted as the positive effect of control variables on the

$\mathcal{S}$ class. Similarly, it is observed that the controls cause an increase in the number of exposed ($\mathcal{E}$) individuals.

In Figure 5, the effect of the established control strategies on the infected and Omicron populations is clearly seen. For example, on the $20th$ day of the simulation process, the number of infected individuals is calculated as $44,237$ and $584,654$ with and without controls, respectively. Similarly, the total number of persons in the Omicron class on the $20th$ day is calculated as $419,776$ and $685,619$ with and without control. This indicates that the control parameters' expected remarkable effect is readily seen.

Owing to efforts to curtail COVID-19 from spreading, we have utilized control $u_1(t)$ in Figure 6. If Figure 6 and Figure 9 are taken into account, a significant decrease is noted in the infected individuals between the $10th$ and $70th$ days, when the control u_1 reaches its maximum value. On the other hand, when Figures 7 and 9 are considered together, the desired positive effect of the control u_2 parameter, which we added to reduce the spread of the Omicron variant, is clearly visible.

In Figure 8, one can see the behaviors of the recovered and heart attack classes under the control parameters. It is observed that the number of individuals who recovered increased due to the presence of the control parameters. In the heart attack class, a decrease is observed with the effect of the control parameters at the beginning. Nevertheless, there is a significant increase in the number of cases of heart attacks observed after the $20th$ day due to the increase in the number of exposed and susceptible individuals over time.

To better evaluate the effectiveness of the control variables under consideration, the cost functional values and reduction percentages were calculated for various strategies and are presented in Table 3.

Table 3. Reduction percentages and values of the cost functional J in (6.1).

Strategy	Value of the cost functional J	Reduction (%)
Without control	$9.07314e+09$	–
$u_1(t), u_2(t)$	$3.57717e+09$	60.57
$u_1(t)$	$5.08637e+09$	43.94
$u_2(t)$	$7.71862e+09$	14.93

As can be seen, with the consideration of $u_1(t)$ and $u_2(t)$ controls together, a reduction of 60.57% in cost functional value occurs. If the $u_1(t)$ and $u_2(t)$ controls are applied separately, it is seen that the reduction rates of 43.94% and 14.93%, respectively, are achieved in the value of the cost functional. Accordingly, we can see that $u_1(t)$ (self-isolation) is a more dominant effect on minimizing the cost function when compared with $u_2(t)$ (treatment).

All of these results are attractive and useful forecasts for COVID-19 and Omicron variant.

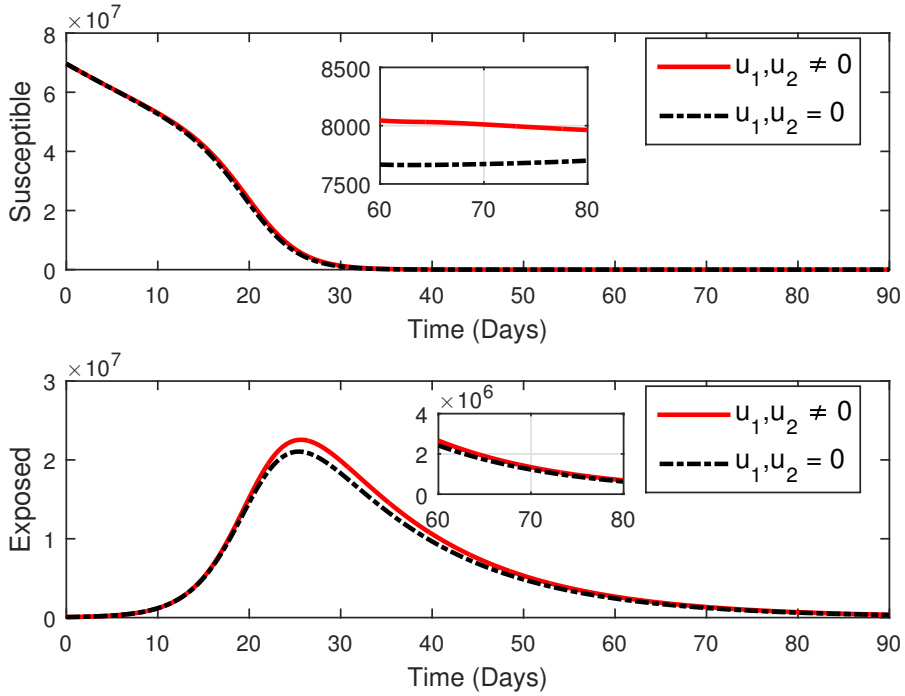

Figure 4. Change of Susceptible and Exposed individuals over time with and without controls.

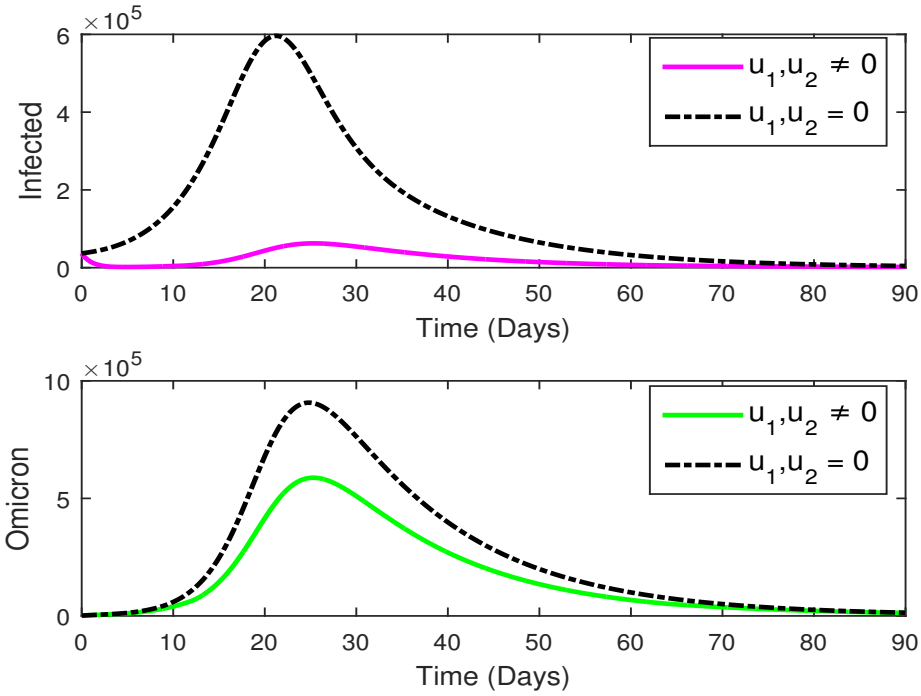

Figure 5. Change of Infected and Omicron individuals over time with and without controls.

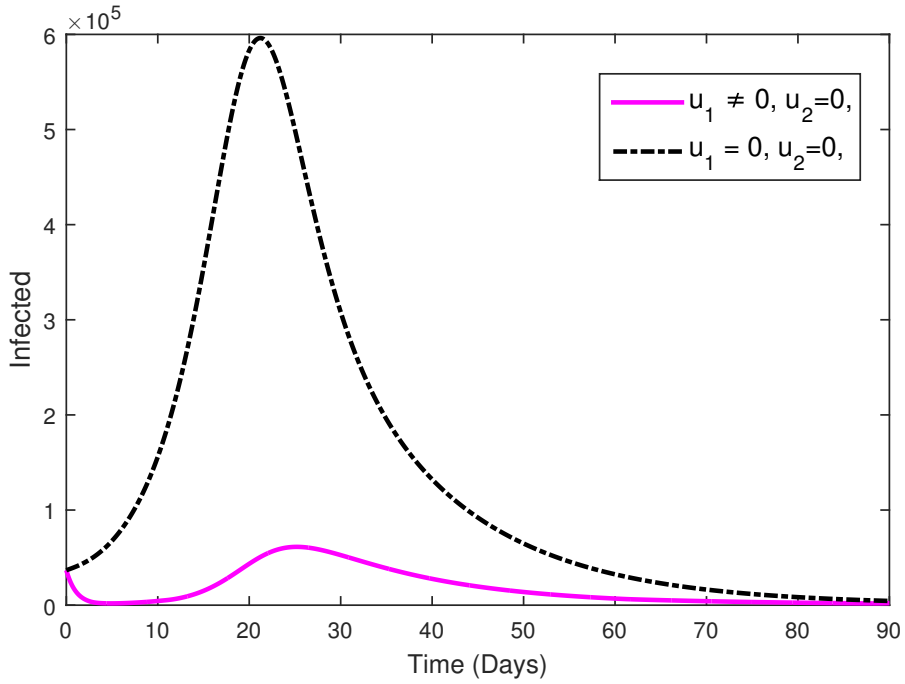

Figure 6. Change of Infected individuals over time with and without control u_1.

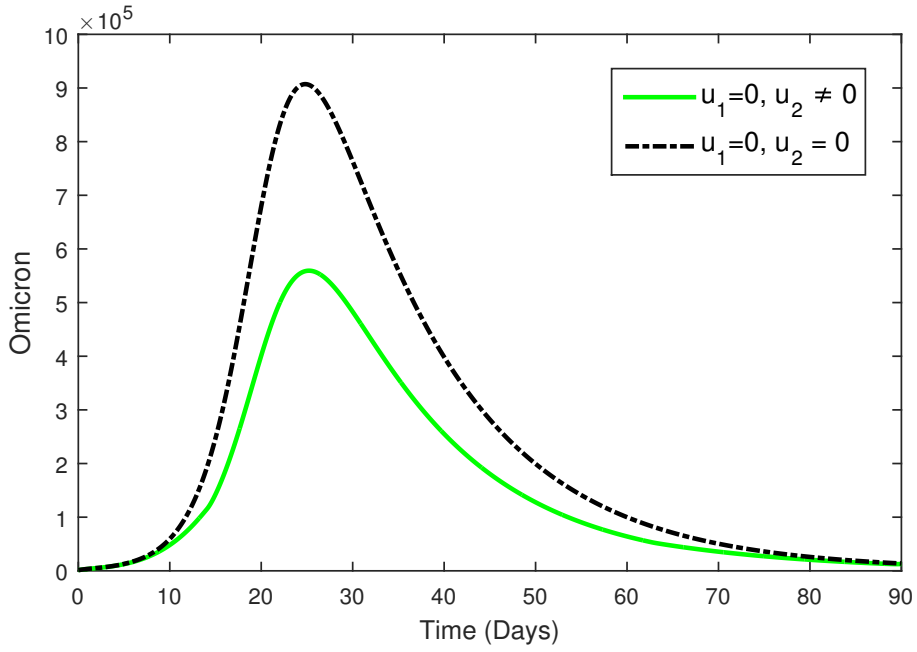

Figure 7. Change of Omicron individuals over time with and without control u_2.

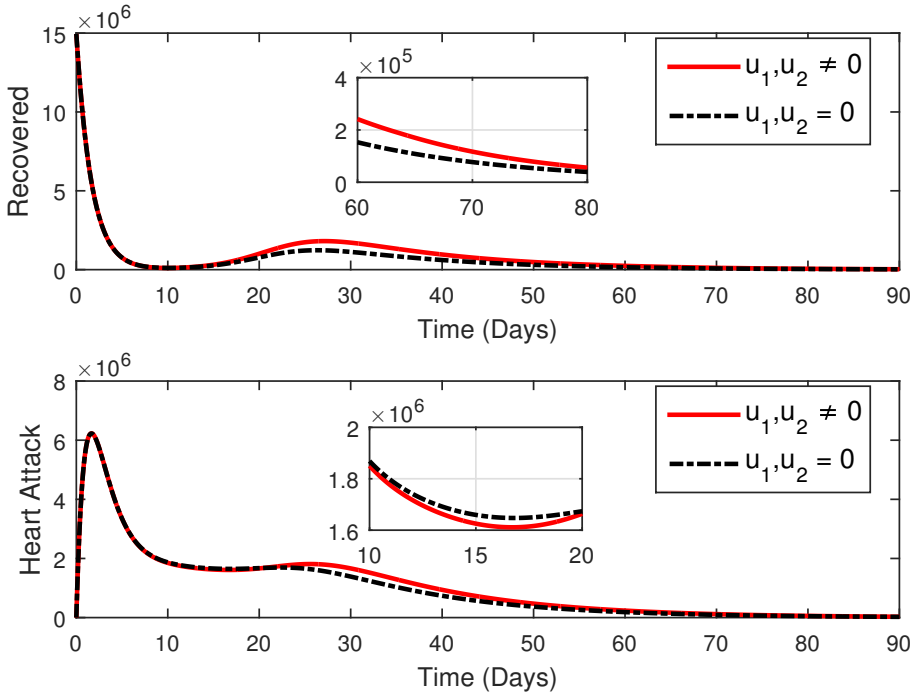

Figure 8. Change of Recovered and Hearth Attack individuals over time with and without controls.

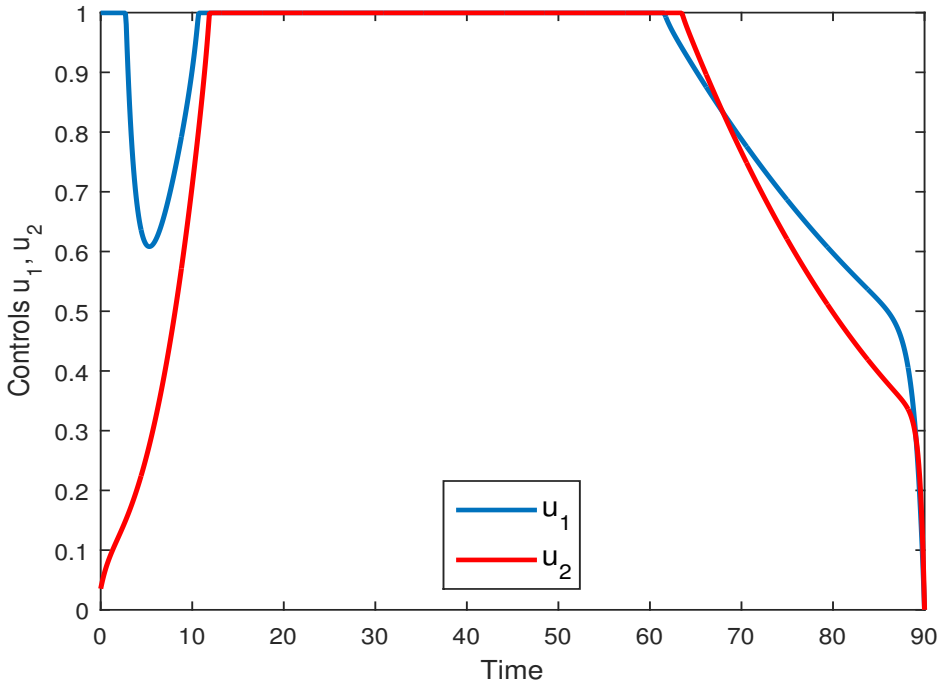

Figure 9. The behaviours of controls u_1 and u_2 over time.

8. Conclusions

In this article, we have studied optimal control strategies on a new COVID-19 and Omicron variant mathematical model with two control parameters as self-isolation $u_1(t)$ and treatment $u_2(t)$. With these control strategies, it is aimed to reduce the number of infected and Omicron individuals.

In the first part of the paper, we demonstrate that the solution to our model is both positive as well as bounded. As well, the NGMM is used to calculate R_0, which is the baseline reproduction number or disease transmission coefficient for the local stability of the disease-free equilibrium. After that, taking into account actual COVID-19 data from Türkiye, LCM was used to minimize the sum of the squares of the difference between the numerical solution provided to the infected persons and the actual data, and the best-fit curve was discovered (see Figure 2). Furthermore, using the parameter estimation (PE) approach, a calibration procedure has been carried out in order to find the most compatible values of the parameters of the model with the goal of better and more realistically observing the disease dynamics. According to specialists in infectious diseases, the Omicron variant of COVID-19 spreads differently from other variants of COVID-19 that have been identified so far [47]. This difference also coincides with the parameter estimation results we have found ($\beta_2 = 0.5$ and $\beta_3 = 0.7$). Furthermore, the level of agreement between the model and the real-data is represented by the absolute relative error in Figure 3. Notably, the fitted model parameters obtained from Figure 3 exhibit biological significance and inspire confidence in their validity.

The sufficient conditions for the control parameters u_1 and u_2 are utilized from Pontryagin's maximum principle. For the numerical simulations of the OCP, the forward-backward sweep method is handled. Numerical simulations in which control strategies are considered separately and together are depicted.

Our results indicate that the control variables lead to a significant reduction in the number of individuals in the infected and Omicron classes, as intended. Based on our investigations, it can be concluded that if infected individuals behave sensitively and self-isolate, and if individuals with the Omicron variant seek proper treatment, it may be possible to decrease and eventually eliminate the disease over time. Furthermore, upon examining Table 3, it becomes clear that self-isolation remains one of the most effective strategies in controlling the spread of COVID-19 and its Omicron variant, even when used alone. Moreover, it has become increasingly urgent to continue practicing self-isolation in order to prevent COVID-19 from undergoing further dangerous mutations.

Use of AI tools declaration

The authors declare they have not used Artificial Intelligence (AI) tools in the creation of this article.

Acknowledgements

F. Özköse was supported by Research Fund of the Erciyes University. Project Number: FDS-2021-11059.

M. Yavuz was supported by TUBITAK and Necmettin Erbakan University Research Grant No. BAP 211215005.

N. Özdemir was supported by Balıkesir University Research Grant No. BAP 2021-121.

Conflict of interest

The authors declare that they have no known competing financial interests or personal relationships that could have appeared to influence the work reported in this paper.

References

1. Mishra P, Parveen R, Bajpai R, et al. (2021) Impact of cardiovascular diseases on severity of COVID-19 patients: a systematic review. *Ann Acad Med Singap* 50: 52–60. https://doi.org/10.47102/annals-acadmedsg.2020367
2. Harrison SL, Buckley BJ, Rivera-Caravaca JM, et al. (2021) Cardiovascular risk factors, cardiovascular disease, and COVID-19: an umbrella review of systematic reviews. *Eur Heart J-Qual Car* 7: 330–339. https://doi.org/10.1093/ehjqcco/qcab029
3. Clerkin KJ, Fried JA, Raikhelkar J, et al. (2021) COVID-19 and cardiovascular disease. *Circulation* 141: 1648–1655. https://doi.org/10.1161/CIRCULATIONAHA.120.046941
4. Naik PA, Eskandari Z, Yavuz M, et al. (2022) Complex dynamics of a discrete-time Bazykin-Berezovskaya prey-predator model with a strong Allee effect. *J Comput Appl Math* 413: 114401. https://doi.org/10.1016/j.cam.2022.114401
5. Sene N (2022) Second-grade fluid with Newtonian heating under Caputo fractional derivative: analytical investigations via Laplace transforms. *Math Model Num Simul Appl* 2: 13–25. https://doi.org/10.53391/mmnsa.2022.01.002
6. Sabbar Y (2023) Asymptotic extinction and persistence of a perturbed epidemic model with different intervention measures and standard lévy jumps. *Bull Biomath* 1: 58–77. https://doi.org/10.59292/bulletinbiomath.2023004
7. Hammouch Z, Yavuz M, Özdemir N (2021) Numerical solutions and synchronization of a variable-order fractional chaotic system. *Math Model Num Simul Appl* 1: 11–23. https://doi.org/10.53391/mmnsa.2021.01.002
8. Naik PA, Yavuz M, Qureshi S, et al. (2020) Modeling and analysis of COVID-19 epidemics with treatment in fractional derivatives using real data from Pakistan. *Eur Phys J Plus* 135: 1–42. https://doi.org/10.1140/epjp/s13360-020-00819-5
9. Joshi H, Yavuz M, Townley S, et al. (2023) Stability analysis of a non-singular fractional-order covid-19 model with nonlinear incidence and treatment rate. *Phys Scripta* 98: 045216. https://doi.org/10.1088/1402-4896/acbe7a
10. Atede AO, Omame A, Inyama SC (2023) A fractional order vaccination model for COVID-19 incorporating environmental transmission: a case study using Nigerian data. *Bull Biomath* 1: 78–110. https://doi.org/10.59292/bulletinbiomath.2023005
11. Uçar S, Uçar E, Özdemir N, et al. (2019) Mathematical analysis and numerical simulation for a smoking model with Atangana–Baleanu derivative. *Chaos Soliton Fract* 118: 300–306. https://doi.org/10.1016/j.chaos.2018.12.003

12. Naik PA, Owolabi KM, Yavuz M, et al. (2020) Chaotic dynamics of a fractional order HIV-1 model involving AIDS-related cancer cells. *Chaos Soliton Fract* 140: 110272. https://doi.org/10.1016/j.chaos.2020.110272

13. Evirgen F, Ucar E, Ucar S, et al. (2023) Modelling influenza a disease dynamics under Caputo-Fabrizio fractional derivative with distinct contact rates. *Math Model Num Simul Appl* 3: 58–72. https://doi.org/10.53391/mmnsa.1274004

14. Uçar E, Uçar S, Evirgen F, et al. (2021) A fractional SAIDR model in the frame of Atangana–Baleanu derivative. *Fractal Fract* 5: 32. https://doi.org/10.3390/fractalfract5020032

15. Elhia M, Balatif O, Boujallal L, et al. (2021) Optimal control problem for a tuberculosis model with multiple infectious compartments and time delays. *IJOCTA* 11: 75–91. https://doi.org/10.11121/ijocta.01.2021.00885

16. Nwajeri UK, Atede AO, Panle AB, et al. (2023) Malaria and cholera co-dynamic model analysis furnished with fractional-order differential equations. *Math Model Num Simul Appl* 3: 33–57. https://doi.org/10.53391/mmnsa.1273982

17. Agarwal P, Nieto JJ, Torres DFM (2022) *Mathematical Analysis of Infectious Diseases*, Academic Press. https://doi.org/10.1016/C2020-0-03443-2

18. Yıldız TA, Arshad S, Baleanu D (2018) New observations on optimal cancer treatments for a fractional tumor growth model with and without singular kernel. *Chaos Soliton Fract* 117: 226–239. https://doi.org/10.1016/j.chaos.2018.10.029

19. Malinzi J, Ouifki R, Eladdadi A, et al. (2018) Enhancement of chemotherapy using oncolytic virotherapy: Mathematical and optimal control analysis. *Math Biosci Eng* 15: 1435–1463. https://doi.org/10.3934/mbe.2018066

20. Yıldız TA (2019) A comparison of some control strategies for a non-integer order tuberculosis model. *IJOCTA* 9: 21–30. https://doi.org/10.11121/ijocta.01.2019.00657

21. Yıldız TA, Karaoğlu E (2019) Optimal control strategies for tuberculosis dynamics with exogenous reinfections in case of treatment at home and treatment in hospital. *Nonlinear Dynam* 97: 2643–2659. https://doi.org/10.1007/s11071-019-05153-9

22. Baleanu D, Jajarmi A, Sajjadi SS, et al. (2019) A new fractional model and optimal control of a tumor-immune surveillance with non-singular derivative operator. *Chaos* 29: 083127. https://doi.org/10.1063/1.5096159

23. Abidemi A, Aziz NAB (2020) Optimal control strategies for dengue fever spread in Johor, Malaysia. *Comput Meth Prog Bio* 196: 105585. https://doi.org/10.1016/j.cmpb.2020.105585

24. Jajarmi A, Yusuf A, Baleanu D, et al. (2020) A new fractional HRSV model and its optimal control: a non-singular operator approach. *Physica A* 547: 123860. https://doi.org/10.1016/j.physa.2019.123860

25. Naik PA, Zu J, Owolabi KM (2020) Global dynamics of a fractional order model for the transmission of HIV epidemic with optimal control. *Chaos Soliton Fract* 138: 109826. https://doi.org/10.1016/j.chaos.2020.109826

26. Ameen I, Baleanu D, Ali HM (2020) An efficient algorithm for solving the fractional optimal control of SIRV epidemic model with a combination of vaccination and treatment. *Chaos Soliton Fract* 137: 109892. https://doi.org/10.1016/j.chaos.2020.109892

27. Elhia M, Balatif O, Boujallal L, et al. (2021) Optimal control problem for a tuberculosis model with multiple infectious compartments and time delays. *IJOCTA* 11: 75–91. https://doi.org/10.11121/ijocta.01.2021.00885

28. Sweilam NH, Al-Mekhlafi SM, Albalawi AO, et al. (2021) Optimal control of variable-order fractional model for delay cancer treatments. *Appl Math Model* 89: 1557–1574. https://doi.org/10.1016/j.apm.2020.08.012

29. Zhao J, Yang R (2021) A dynamical model of echinococcosis with optimal control and cost-effectiveness. *Nonlinear Anal Real World Appl* 62: 103388. https://doi.org/10.1016/j.nonrwa.2021.103388

30. Mohammadi H, Kumar S, Rezapour S, et al. (2021) A theoretical study of the Caputo–Fabrizio fractional modeling for hearing loss due to Mumps virus with optimal control. *Chaos Soliton Fract* 144: 110668. https://doi.org/10.1016/j.chaos.2021.110668

31. Abbasi Z, Zamani I, Mehra AHA, et al. (2020) Optimal control design of impulsive SQEIAR epidemic models with application to COVID-19. *Chaos Soliton Fract* 139: 110054. https://doi.org/10.1016/j.chaos.2020.110054

32. Moussouni N, Aliane M (2021) Optimal control of COVID-19. *IJOCTA* 11: 114–122. https://doi.org/10.11121/ijocta.01.2021.00974

33. Nabi KN, Kumar P, Erturk VS (2021) Projections and fractional dynamics of COVID-19 with optimal control strategies. *Chaos Soliton Fract* 145: 110689. https://doi.org/10.1016/j.chaos.2021.110689

34. Arruda EF, Das SS, Dias CM, et al. (2021) Modelling and optimal control of multi strain epidemics, with application to COVID-19. *Plos One* 16: e0257512. https://doi.org/10.1371/journal.pone.0257512

35. Tchoumi SY, Diagne ML, Rwezaura H, et al. (2021) Malaria and COVID-19 co-dynamics: A mathematical model and optimal control. *Appl Math Model* 99: 294–327. https://doi.org/10.1016/j.apm.2021.06.016

36. Araz SI (2021) Analysis of a Covid-19 model: optimal control, stability and simulations. *Alexandria Eng J* 60: 647–658. https://doi.org/10.1016/j.aej.2020.09.058

37. Rosa S, Torres DFM (2022) Fractional modelling and optimal control of COVID-19 transmission in Portugal. *Axioms* 11: 170. https://doi.org/10.3390/axioms11040170

38. Fatima B, Yavuz M, ur Rahman M, et al. (2023). Modeling the epidemic trend of middle eastern respiratory syndrome coronavirus with optimal control. *Math Biosc Eng* 20: 11847–11874. https://doi.org/10.3934/mbe.2023527

39. Özköse F, Yavuz M (2022) Investigation of interactions between COVID-19 and diabetes with hereditary traits using real data: a case study in Turkey. *Comput Biol Med* 141: 105044. https://doi.org/10.1016/j.compbiomed.2021.105044

40. Driessche VP, Watmough J (2002) Reproduction numbers and sub-threshold endemic equilibria for compartmental models of disease transmission. *Math Biosci* 180: 29–48. https://doi.org/10.1016/S0025-5564(02)00108-6

41. Diekmann O, Heesterbeek JAP, Roberts MG (2010) The construction of next-generation matrices for compartmental epidemic models. *J R Soc Interface* 7: 873–885. https://doi.org/10.1098/rsif.2009.0386

42. Chitnis N, Hyman JM, Cushing JM (2008) Determining important parameters in the spread of malaria through the sensitivity analysis of a mathematical model. *Bull Math Biol* 70: 1272. https://doi.org/10.1007/s11538-008-9299-0

43. Coddington EA, Levinson N (1955) *Theory of Ordinary Differential Equations*, Tata McGraw-Hill Education.

44. Gaff HD, Schaefer E, Lenhart S (2011) Use of optimal control models to predict treatment time for managing tick-borne disease. *J Biol Dynam* 5: 517–530. https://doi.org/10.1080/17513758.2010.535910

45. Pontryagin LS (1987) *Mathematical Theory of Optimal Processes*, 1 Ed., CRC Press. https://doi.org/10.1201/9780203749319

46. Lenhart S, Workman JT (2007) *Optimal Control Applied to Biological Models*, 1 Ed., CRC Press. https://doi.org/10.1201/9781420011418

47. Vitiello A, Ferrara F, Auti AM, et al. (2022) Advances in the Omicron variant development. *J Int Med* 292: 81–90. https://doi.org/10.1111/joim.13478

AIMS Press